Journal of Materials Science: Materials in Electronics (2020) 31:11927–11937
https://doi.org/10.1007/s10854-020-03747-3

Synthesis of silver nanoparticles decorated on reduced graphene oxide nanosheets and their electrochemical sensing towards hazardous 4-nitrophenol

Naushad Ahmad[1] · Ahmed S. Al-Fatesh[2] · Rizwan Wahab[3] · Manawwer Alam[1] · Anis H. Fakeeha[2]

Received: 21 April 2020 / Accepted: 5 June 2020 / Published online: 11 June 2020

Abstract
In this study, an electrochemical sensor for the detection of 4-Nitrophenol (referred to as 4-NP) was developed based on templated silver nanoparticles (AgNPs) on reduced graphene oxide (rGO) nanosheets (Ag-rGO) and utilized as an electrocatalyst. It was found that the resulting composite exhibits enhanced catalytic activity towards the reduction of 4-NP. The cubic shaped AgNPs templated on rGO nanosheets has been successfully fabricated by a chemical reduction method using sodium borohydride ($NaBH_4$), and it was well characterized through morphological and electrochemical techniques: Ultraviolet–Visible spectroscopy (UV -Vis), scanning electron microscopy (SEM) equipped with energy-dispersive spectroscopy (SEM–EDS), transmission electron microscopy (TEM), X-ray diffraction (XRD), Fourier transform infrared spectroscopy (FT-IR), cyclic voltammetry (CV), and chronoamperometry. The obtained results revealed that the AgNPs scattered on rGO sheets are spherical in shape, and it's estimated to be a dimension of ~ 60 nm in size. The prepared crystalline Ag-rGO nano sheets were further applied as an electrode material for the electrochemical examination with three electrode system to sense the hazardous material 4-NP in PBS. The electrochemical studies were conducted through CV under the condition of bare and coated electrode (Ag-rGO/GCE) with influence of concentration (4-NP from 2 to 150 mM), scan rate, reproducibility (RSD-2.87%) and stability test (4-NP-20 µM) were examined. The data reveal that the Ag-rGO/GCE exhibit highly reproducible and sustainable for the reduction of toxic 4-NP. The chronoamperometry study for current and time response was also studied at two different potentials (− 0.3 V & − 0.6 V), respectively.

1 Introduction

Over a decades nitroaromatic compounds particularly nitrophenols (NP) are widely utilized in many industrial and agricultural sectors as a precursor for phenetidine, acetophenetidine, pesticides, peptides, explosive, dyes, and pharmaceuticals [1, 2]. Out of these nitrophenols, 4-NP is frequently used for the production of these chemicals [1]. Besides their valuable application, it has been considered as anthropogenic, toxic, inhibitory, and bio-refractory compounds and it causes adverse effects on health such as headaches, drowsiness, nausea, cyanosis, methemoglobinemia, fervescence, damage of liver and kidney by ingestion/inhalation [3–5]. The hazardous compounds nitro phenol can damage the crop, water bodies and environment when released in to the soil [3–8]. Because of their heavier toxicity rate, even at a very trace level, its listed in US Environmental Protection Agency (USEPA) and the maximum recommended value in effluents is set to less than 700 µM [9].

Thus, it's an urgent need to develop techniques, which can detect very fast, at a very low detection limit, selective, handy, simple operation and cost effective to detoxify and convert in to small organic chain to degradate 4-NP. Among various well established methods mentioned in the literature [10–13], electrochemical techniques offer the economic opport- unity for rapid detection of 4-NP and also other hazardous chemicals [8, 14–17]. Several strategies

✉ Naushad Ahmad
anaushad@ksu.edu.sa

✉ Rizwan Wahab
rwahab@ksu.edu.sa

[1] Department of Chemistry, College of Science, King Saud University, Riyadh 11451, Kingdom of Saudi Arabia

[2] Chemical Engineering Department, College of Engineering, King Saud University, Riyadh 11421, Kingdom of Saudi Arabia

[3] Department of Zoology, College of Science, King Saud University, Riyadh 11451, Kingdom of Saudi Arabia

have been applied on the electrode surfaces to get high sensitivity, reproducible result and reduced over potential for 4-NP reduction. The surface of the electrode can be modify with reliable tactic for accelerate the rate electron transfer process and to minimize the over potential. Many research groups are well established electrochemical redox mediator using noble metals, oxide of metals, and mixed metal oxide for detection of 4-NP and relatively obtained a wide range of linear detection as compared to the unmodified electrodes and modified by macrostructured molecules [7, 8, 14–17].

Nowadays, carbon based nanomaterials having a different kind of morphology and is believed to provide a new path for the development of high performance electrochemical sensors due to their enhanced-renewable-rich surface chemistry, good electron transport property and low residual current and wide potential window [3–6, 18–21]. Two more importantly and structurally different carbon nanostructured: carbon nanotubes and graphene are fundamentally and practically very useful for the detection of 4-NP because they developed efficient interfacial relationship, which are largely assist in electron transport properties. Efforts from past decades, it has been investigated that of these carbon families, graphenes are great concern from the electrochemical point of view and provides much better opportunity and reactivity towards chemical species because of its good conductivity, mechanical stability and its two-dimensional (2D) tightly packed honeycomb structure can be tuned, wrapped, rolled or stacked into other dimensional structure such nanotubes (1D), graphite (3D) or fullerenes (0D) as compared to other carbonaceous materials [22–27]. Thus, the graphene and their derivative, which is tightly bonded with oxygen and termed as graphene oxide (GO) and ideal material. The GO is a most desirable, suitable source material for the preparation of metal based graphene NPs composites, paid to their unique benefits for instance cost effective, easy to produce from the graphite, good electronic properties through NPs, easy to process in an aqueous medium and exhibit sites for functionalization etc. [28–39]. In the literature, noble metal NPs, mixed metal oxide have been studied as electrocatalysts for the reduction of 4-NP. Whereas, the graphene oxide (GO), reduced graphene oxide (rGO) structures not much explored for the development of electrochemical sensors [28–39].

Considering the exceptional properties and enhanced electrochemical output of graphene and its derivative, we reported here, the electrochemical reduction of 4-NP by silver NPs decorated on reduced graphene oxide (Ag-rGO) based sensor. The Ag-rGO was processed through the reduction $NaBH_4$ and utilized as a reformed glassy carbon electrode (GCE). Further, the fabricated two-dimensional sensors were characterized by various analytical, morphological and electrochemical techniques for the investigation of crystal structure, morphology, and optical catalytic properties.

2 Experimental

2.1 Materials

Sliver nitrate ($AgNO_3$, 98.99%), Sodium borohydride ($NaHB_4$, 98.99%), and 4-nitro phenol (4-NP) were purchased from D.F. Goldsmith-Producer & distributers of precious metals (USA); and Graphene oxide (GO) was recovered from Sigma Aldrich (999.99%, USA). Monosodium di-hydrogen phosphate (NaH_2PO_4), disodium monohydrogen phosphate (Na_2HPO_4) were obtained from Aladin Ltd. (Shanghai, China) and used as received. The water used throughout experiments was purified through a Millipore system. Phosphate buffer saline (PBS) was prepared daily by mixing stock solutions of NaH_2PO_4 and Na_2HPO_4 in DI water.

2.2 Characterization

Numerous techniques were applied to identify the processed material such as X-ray diffraction pattern (XRD, Rigaku, Japan) analysis was employed for to know the particles size materials, phase and crystallinity of rGO and Ag-rGO nanosheets with copper K_α radiation ($\lambda = 0.1540$ nm). The materials functional characteristic were evaluated through Fourier transform infrared spectra (FT-IR, Bruker Vector-22) with using KBr pellets ranges from 400 to 4000 cm^{-1}. The thermal stability of the material was analyzed through Thermo gravimetric analysis (TGA, STA Jupiter 449 equipment (Netzsch, Germany)) and carried out in the temperature range from 50 to 1000 °C with heating rate of 20 °C/min, under nitrogen environment with using α-Al_2O_3 as a reference material. The optical characteristic of the material was examined through UV–Visible spectroscopy (UV-2550, Shimadzu, Japan). For this the formed material was completely dissolved in double distilled water and diluted well. The spectra were observed in the range of 200–800 nm with a UV Visible spectrophotometer. The particle diameter, polydispersity index (PDI) and Zeta (ξ) potential of samples were determined by dynamic light scattering (DLS) by Zeta Sizer-HT (Malvern, UK). For this analysis, the samples were suspended in deionized ultrapure water to obtain a concentration of 50 mg/mL, and sonicated at 40 W for 30 min. The samples were sieved via 0.2 mm and the clear NPs solution was used and measurement was accessed at the respective range. The scanning electron microscopy (SEM, JEOL JSM-6380LV, Japan) was utilized for to check the formed powder particles structural dimension enbuild with an energy-dispersive X-ray spectrometer (EDS). Furthermore, for more detail evaluation

of the materials structural detail, the transmission electron microscopy (TEM, HITACHI H-8100 Hitachi, Tokyo, Japan) measurements were conducted with an accelerating voltage of 80 kV. The sample for TEM characterization was prepared by placing a drop of colloidal solution on carbon-coated copper grid and dried at room temperature. The dried carbon-coated grid was further fixed with the sample holder and analyzed the structural measurement. The electrochemical studies were performed with a Metrohm Autolab analyzer (PGSTAT30, Switzerland). The arrangement of three three-electrode cell system was used with a glassy carbon electrode (GCE, geometric area = 7×10^{-2} cm^2). To this defined area the prepared Ag-rGO nanosheets were deposited as described above and used as a working electrode, reference electrode Ag/AgCl (saturated KCl), and platinum foil were utilized as a counter electrode. The potentials are measured with a Ag/AgCl electrode as the reference electrode. All the experiments were conducted in an ambient atmosphere.

2.3 Formation of silver doped reduced graphene oxide (Ag-rGO)

The dispersion of rGO was formed by the use of chemical reduction of GO with $NaBH_4$ as a reducing agent. For this, about 50 mg of GO nanosheets were sonicated in 20 mL of distilled water and to kept 30 min to get a stable dispersion and to add ~ 10 mL of a freshly prepared solution of $NaBH_4$ (1 mM). From this prepared solution, the 18 ml of 1 mM $AgNO_3$ solution was mixed and sonicated further for additional 15 min. The whole mixture was well sonicated (~ 10–15 min) and thereafter, transferred in a beaker and to preserve for 12 h at room temperature, a green Ag-rGO precipitate was obtained. The recovered precipitate was washed thoroughly with Milli-Q water and centrifuge at 6000 rpm for 30 min, and dried in an oven at 85 °C.

2.4 Fabrication of Ag-rGO/GCE modified working electrode

At initial the GCE was polished with 0.05 mm alumina slurry and Buehler polishing cloth, thereafter washed with DW and sonicated for about 5 min in water and ethanol (EtOH), to remove the any dirt or particles adsorbed on the surface and dried. Once it was cleaned well the electrode was fabricated with the use of Ag-rGO (5 µL) deposited as drop-casting process on to the GC electrode surface and allowed it to dry at 60 °C for 2 h in an oven. The fabricated electrode was used as sensor for the electrochemical detection studies against the 4-NP.

3 Results and discussion

3.1 X-ray diffraction (XRD) of Ag-rGO nanosheets

Figure 1 describes the X-ray diffraction pattern of rGO and Ag-rGO nanosheets. The rGO displays a sharp diffraction peak at 26.1° in XRD profile which is assigned for (002) plane [40–42]. The interlayer spacing of rGO was 0.35 nm, slightly larger than that of graphite and fabricated composite (0.34 nm). The as-synthesized silver decorated rGO shows four peaks at 2θ = 38.08°, 43.96°, 64.10° and 77.24° which are assigned for (111), (200), (220), (311) planes of crystalline face-centered cubic (fcc) AgNPs, respectively [43]. The (111) plane of AgNPs (JCPDS No. 04-0783), indicates that the NPs are composed of pure crystalline silver. The phase (004) at 54.3° denotes the formation of graphene sheets, which is evident in both rGO and composite Ag-rGO [44]. The XRD data justify that the AgNPs were effectively loaded onto the rGO nanosheets.

3.2 FT-IR study

The FT-IR observation for the rGO and AgNP are illustrated as Fig. 2, which shows the chemical characteristics of AgNPs and rGO. The spectrum of rGO exhibits a broad peak at 3400 cm^{-1}, ascribed to the intercalated water molecules [45], whereas the peaks at 2919, 1717, 1615, 1411, 1378 and 1108 cm^{-1}, suggest the presence of C–H, C=O, C=C, C–OH, C–O–C and C–O groups, respectively [46]. In this experiment, there is no peak related to the C–OH at 1230 cm^{-1} stretching mode were observed, which further confirm the formation of rGO. Very similar characteristic of absorption was also observed for Ag-rGO composite and

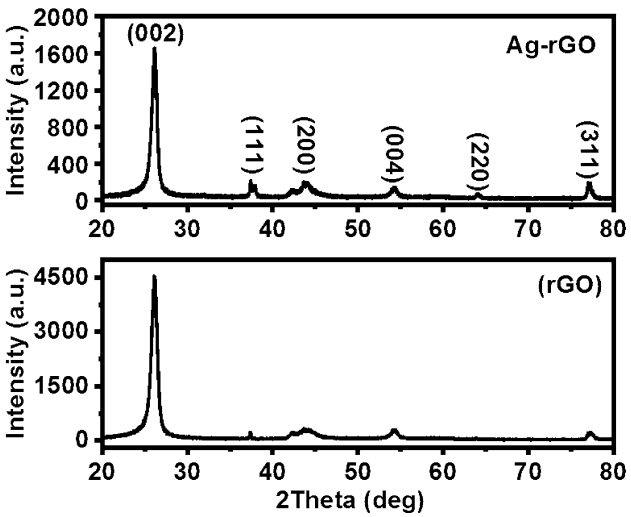

Fig. 1 XRD patterns for rGO and Ag-rGO nanosheets

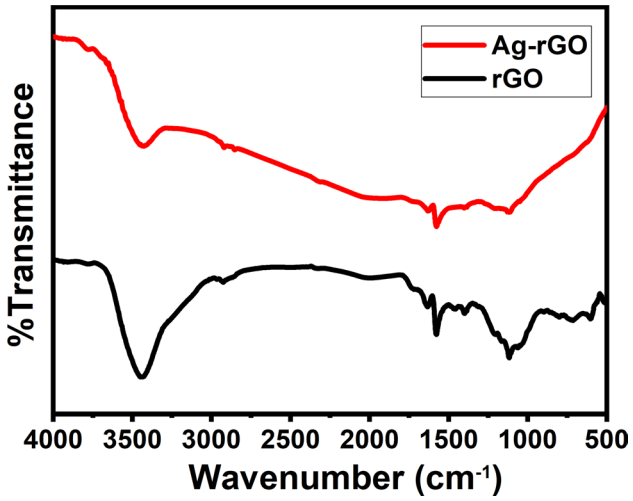

Fig. 2 FT-IR spectra of rGO and Ag-rGO nanosheets

it denotes that the presence of Ag does not influence the rGO. On The obtained data again indicate the formation of nanocomposite. Typically, the FT-IR peaks belonging to the rGO either disappear or their intensities are significantly reduced after the reduction process, which in turn confirms the formation of AgNPs modified rGO. The broad band at 3443 cm^{-1} for hydroxyl groups shows the reduction of rGO to Ag-rGO.

3.3 Thermal study (Thermogrivimetric analysis)

Figure 3 showed the TGA curves of rGO and its silver composite. In both, the mass loss decompositions are observed above 300 °C and rGO shows higher thermal stability as compared to Ag-rGO. In rGO, total mass loss is around 10% while in Ag-rGO is 50%. Ag-rGO nanosheets represents two decompositions: the first mass loss (10%) was observed upto 300 °C due to removal of physically adsorbed water molecule, and the second mass loss (40%) displayed above 300 °C upto mostly decomposition of oxygen containing functional groups like hydroxide, alcohols, carbonyl, esters and lastly nitrates of sodium and silver. At the end of decomposition, there are no any kinds of residual of nitrates and organic compounds, confirmed that the high purity and stability of fabricated materials.

3.4 UV–Visible and dynamic light scattering analysis

Figure 4 shows the UV–Vis absorption spectra of rGO and Ag-rGO nanocomposites. The observed peak at 279 nm denotes the absorption band and it's attributed the reduction of GO which deals the π–π* transitions of aromatic C=C bonds [47]. The absorption peak at 279 nm in rGO was red-shifted to 307 nm (4.03 eV), suggesting the reduction of Ag ions and the formation of Ag-rGO nanocomposite.

As described in the characterization section the DLS was utilized to get the particle size in liquid medium/hydrodynamic size, polydispersity index (PDI) and surface zeta potential of the rGO and Ag-rGO. The hydrodynamic size distribution and Zeta (ξ) potential of fabricated NPs are shown in Fig. 5. It is observed that the particle size of rGO (300 nm) is larger than its silver composite (60 nm) in DI water, (Fig. 5a and c). Because the NP in aqueous suspension have a tendency of agglomeration to make primary and secondary size. Because of agglomeration, the NPs size was differing from TEM to DLS may be the reason of particles agglomeration. Furthermore, the zeta potential of the NPs of rGO and Ag-rGO were found at − 29.75 and − 33.05 V,

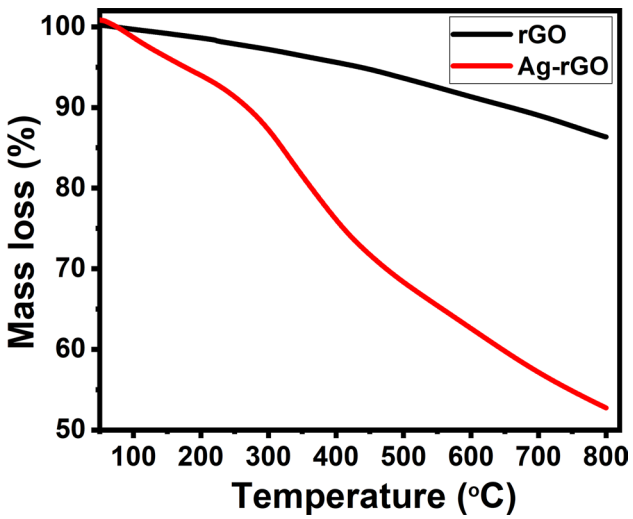

Fig. 3 TGA curves of rGO and Ag-rGO nanosheets

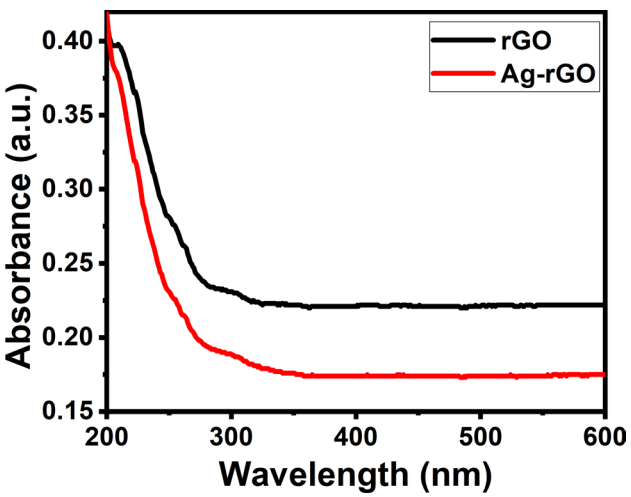

Fig. 4 UV–Vis spectra of rGO and Ag-rGO nanosheets

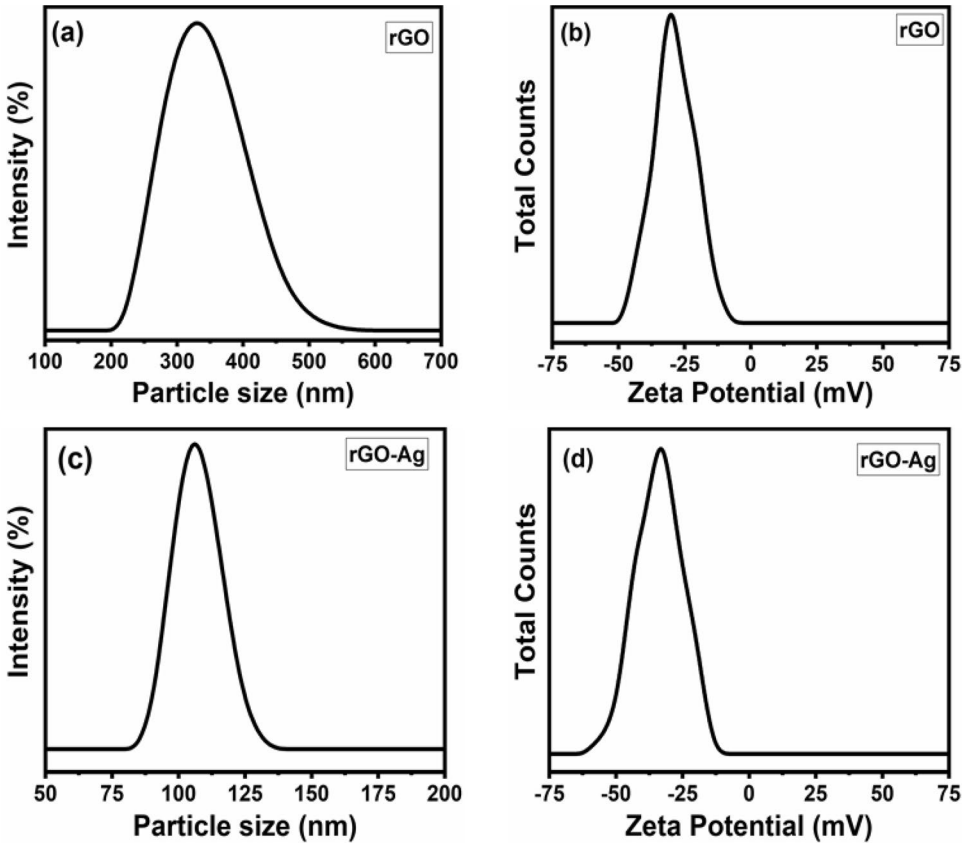

Fig. 5 Particle size and zeta potential of rGO (**a**, **b**) and Ag-rGO (**c**, **d**) nanosheets

respectively (Fig. 5b and d). The negative values of zeta potential were specified the good stability, well dispersed and might be presence of secondary size [48]. The enhance rate of zeta potential signifies a high electrical charge, developed on the surface of the NPs and can develop a strong repellent force with the particles to prevent agglomeration [49, 50]. The PDI values of rGO and its composite was found 0.623 and 1, respectively. Here if the PDI value '0' signifies monodisperse distribution whereas the value '1' denotes poly- disperse distribution [49, 50].

3.5 Morphological analysis of rGO-Ag nanosheets

The structural description of rGO and Ag-rGO were accessed through scanning electron microscopy (SEM). Figure 6a–d shows the SEM images at different magnifications (Fig. 6a–b), confirm the presence Ag on the rGO nanosheet surfaces, and the immobilized particles are spherical in shape. Invariance, rGO reveals randomly aggregated and oriented as thin, rippled, crumpled and entangled with each other (Fig. 6a–c). The sheets are seems to be transparent and lateral in dimensions with ranged from 100 nm to several μm [51, 52]. It's very clear from the images (Fig. 6d) that the rGO sheets that are highly decorated with spherical Ag particles (Fig. 6d), and shows good interactions between Ag and rGO. The surface attached Ag particles are spherical in shape with an average diameter ranges from 25 to 60 nm (Fig. 6d inset). From the images, it's evident that the distribution of AgNPs on the surface of rGO is irregular. The irregular nanocrystals agglomerates tethered to rGO surface arise as the repulsive interactions, which are dominated through weak Van der Waals forces of attraction and Brownian motion [51, 52]. The composition of rGO and AgNPs were analyzed from the SEM equipped EDX with a specified area and presented as Fig. 7. The EDX diagram (Fig. 7a and b) confirmed that the white spots of AgNP (Fig. 7a) and its conform that the composition of Ag-rGO sheets like structures exhibit mostly of C and O, but also the Ag element with atomic ratios 10.89, 80.50 and 8.61%, respectively (Fig. 7b). Based on the received results such as X-ray diffraction pattern, FT-IR, TGA, UV–Visible absorption spectro -scopy, DLS and zeta potential, it discloses that the presence of AgNPs act as a template material for rGO.

Detailed morphology and structural features of the Ag-rGO sample was further analyzed through electron microscopy (TEM) measurement. The corresponding result is shown that the graphene sheets overlap with each other and thus it behaves as a three-dimensional network. From the recovered images (Fig. 8a and b), it seems that the graphene sheets are decorated with cubic shaped silver particles included an edge size of 100–250 nm. These cubic crystals are distributed randomly on the surface and edges

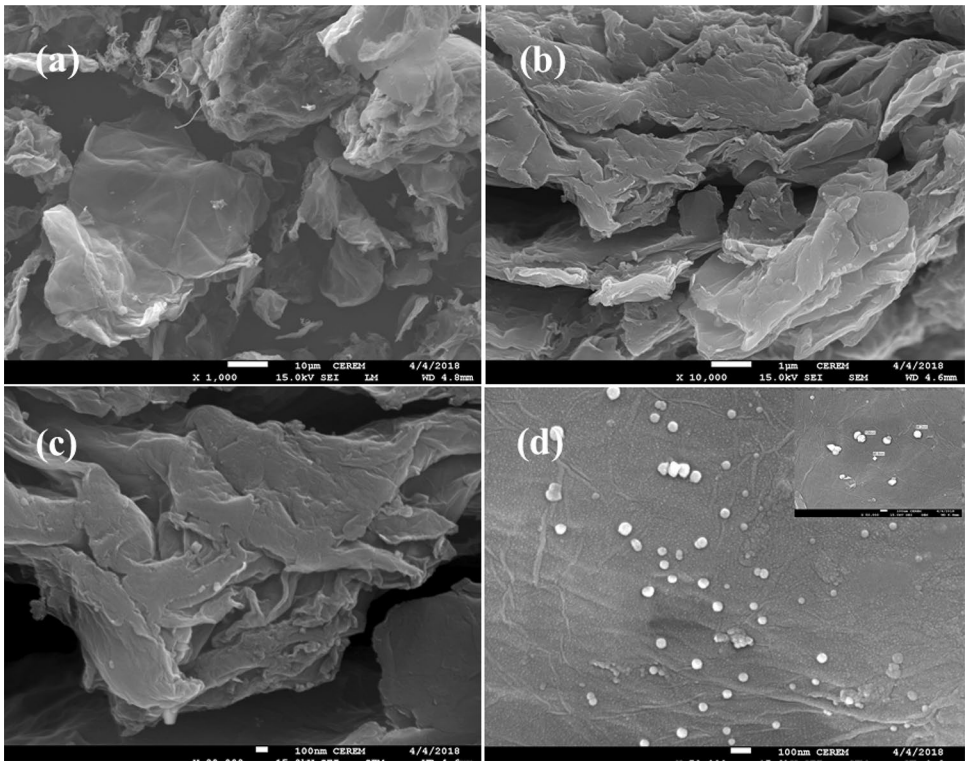

Fig. 6 SEM images Ag-rGO nanosheets at low (**a**–**b**) and high (**b**) magnification, whereas (**d**) shows the AgNPs templated on rGO nanosheets and inset display the size of NPs

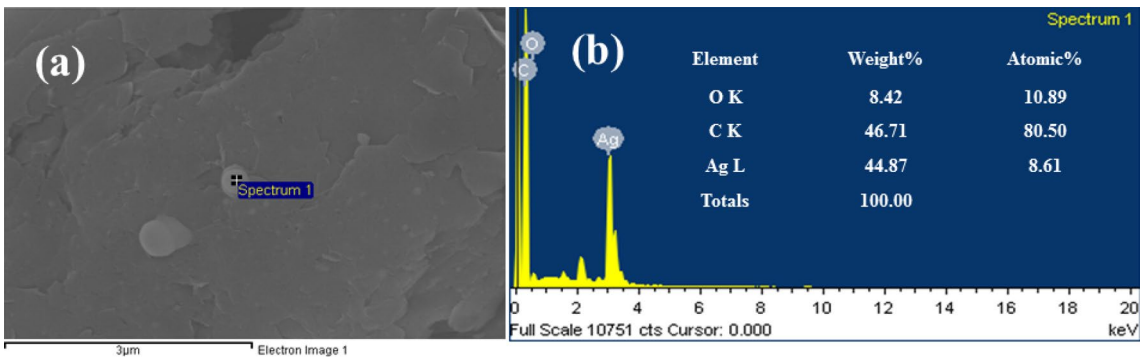

Fig. 7 **a** Shows the SEM image specified area to capture EDX spectra and **b** displayed the elemental atomic ratios of C, Ag and O, respectively

of the graphene sheets, just like the particles adhering to Scotch tape (Fig. 8a). Moreover, the highly crumpled and folded graphene nanosheets with dense edge planes were observed. The dark nanoparticles are observed and cannot be distinguished to each other (Fig. 8a), represent the formation of poly-dispersed AgNPs well accommodated on the GO matrix with a wide particle size distribution varying from 25 to 60 nm. The high magnified image clarifies wide particle size distribution varying from 25 to 60 nm (Fig. 8b). Several small AgNPs are also appear in TEM image of Ag-rGO with dissimilar shape including spherical, twinned structure, triangles etc. (Fig. 8b and inset).

3.6 Electrochemical activity of 4-NP

3.6.1 Electrochemical determination of 4-NP

The bare and modified electrode in presence and absence of 4-NP with 0.1 M PBS, scan rate of 100 mVs^{-1} are presented in Fig. 9. From the obtained spectra it shows that in absence of 4-NP no peaks were observed at bare GCE, but in presence of 4-NP at modified electrodes (GCE/rGO-Ag) peaks are observed. The cathodic peak (Ipc) was observed in the absence and presence of 4-NP (4 µM) at potential of −0.46 and −0.49, respectively, thus hybrid of AgNP/

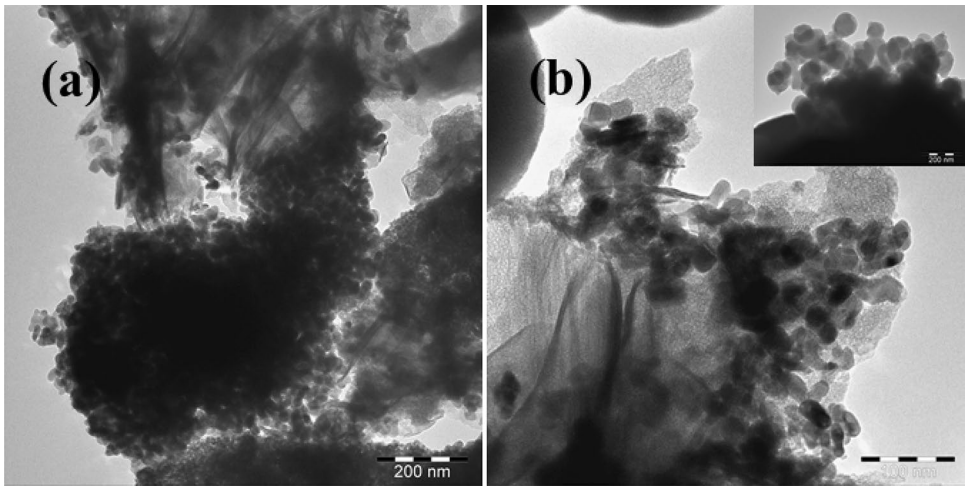

Fig. 8 TEM images with low (**a**) and high (**b**) magnifications of Ag-rGO nanosheets. Also inset (**b**) show the surface attached particles of AgNPs on rGO nanosheets

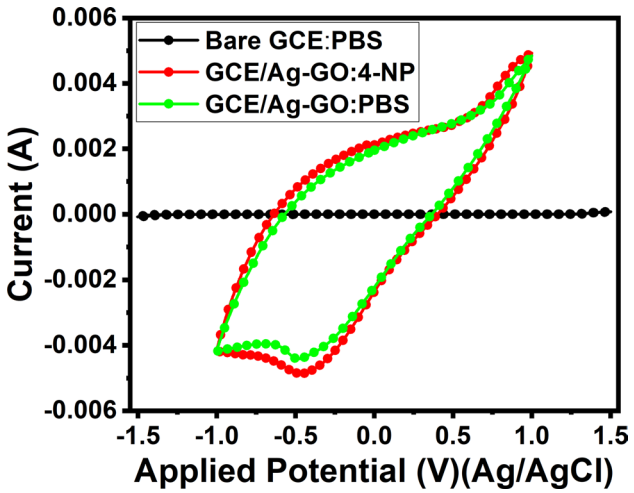

Fig. 9 Cyclic voltammograms of bare and modified electrodes in the absence and presence of 4-NP (4 µM) in 0.1 M phosphate buffer (pH 7.4). Scan rate: 100 mVs^{-1}

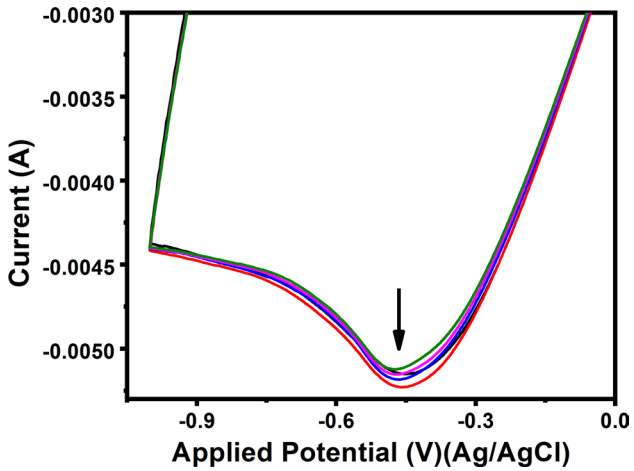

Fig. 10 Cyclic voltammetric responses of Ag-rGO nanosheets in 0.1 M phosphate buffer at different concentrations (2, 30, 70,120 and 150 µM) of 4-NP

rGO is improved the electrical conductivity and transferability of electron. From the obtained graph it is also clear that reaction is completely irreversible reduction in both cases, as confirmed by the absence of an anodic peak. And GCE/rGO-Ag electrode in presence of 4-NP exhibited substantially higher current (− 4.98 mA) as compared to absence of 4-NP (− 4.43 mA) due to the high surface ratio, enhanced conductivity with fast electron transfer rate, again justifies the crucial role of the reduced graphene sheets in the electrocatalytic detection towards the reduction of 4-NP. Based on the required results, the GCE/rGO-Ag electrode showed a synergistic effect with the combination of AgNP and it reduces the graphene sheets on the electrochemical reduction of it. It is known that the reduction of the Ar–NO_2 group of 4-NP produces Ar–NHOH as the product through a single-step, four-electron transfer process in a phosphate buffer with pH 7.2 [53].

3.6.2 Influence of concentration and scan rate variation of 4-NP

Figure 10 shows the CVs of GCE/rGO-Ag electrode with a series of concentration of 4-NP (2 to 150 µM) in N_2-saturated 0.1 M PBS (pH 7.4). Moreover, upon the addition of 4-NP into the electrolyte, the current increase with the increase of 4-NP concentration and peak potential little shifted positively. The voltammetric studies indicate that the as-synthesized GCE/rGO-Ag can effectively electro catalyze to 4-NP reduction.

Figure 11a shows the scan rate of formed Ag-rGO/GCE electrode in presence of 4-NP (4 µM). In our result, the cathodic peak current (Ipc) rise linearly with increasing scan

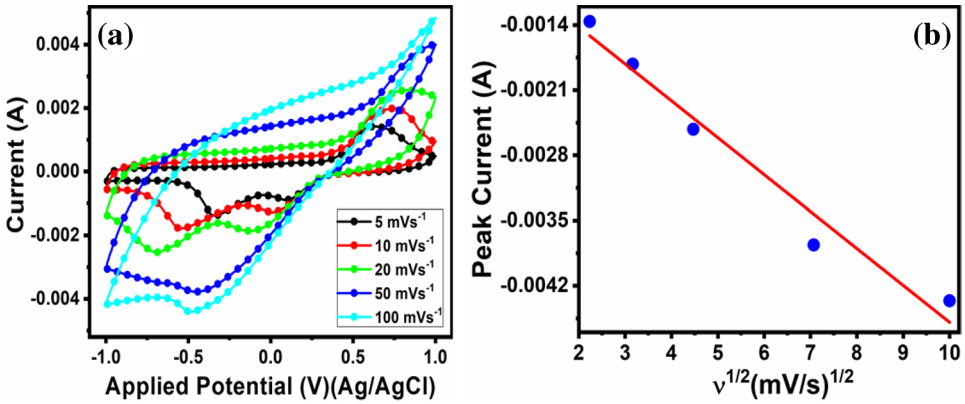

Fig. 11 **a** Cyclic voltammetric responses of Ag-rGO nanosheets in the presence of 4-NP (4 µM) as a function of scan rates and **b** Linear calibration curve

rate from 5 to 100 mV/s, such characteristic shows the a surface-confined electrode process; the potential of cathodic peak moved in a positive direction at their higher scan rate and negative at lower scan rate, respectively. The linear data for Ipc of scan rate are presented as Fig. 11b. The linear regression equation for the reduction process of 4-NP can be written as Ipc = − 3.9 6E−4ν − 6.28E−4; R^2 = 0.968, where, n is the scan rate. The obtained results are kinetically controlled by diffusion process and it's clearly justified that the electrostatic interaction are developed between the electrode and 4-NP [54, 55]. Also, the AgNPs gave more surface area with the surface electrostatic interaction of exposed AgNPs with 4-NP molecules causing enhanced electron transfer and improvement in the electrochemical reduction of 4-NP.

3.6.3 Reproducibility and stability

To evaluated the sensing properties of fabricated electrode reproducibility and stability were investigated in presence of 4-NP (20 µM) in 0.1 M PBS. Figure 12a and b shown the five parallel reproducible cycles and stability, respectively of electrode. The reproducibility of sensor (Ag-rGO/GCE) displayed an excellent result in a five consecutive measurements with 4-NP (Fig. 12a). The relative standard deviation (RSD) was found 2.87%, again confirm that the modified sensor is satisfactory reproducible. In addition to this, the stability of the sensor (Ag-rGO/GCE) was further also evaluated (Fig. 12b).The stability tests was carried out in one and after 15 days, during this period the sensor was stored at an ambient conditions and it doesn't reflect any change in curve of voltammetric cycle with a difference of the reduction current of ~ 13.38% as associated with its initial value, further confirm their long storage stability. These results show that Ag-rGO on GCE surface has appreciable reproducibility and stability for the reduction of toxic 4-NP.

4 Chronoamperometry study

The chronoamperometric measurment is largely employed to know the activity and stability of the catalyst. The chronoamperometric measurements for the fabricated Ag-rGO/GCE are shown in Fig. 13 to compare the catalytic stability at − 0.3 V and − 0.6 V, respectively, in 0.1 PBS by successive addition of 4-NP at 5 µL under stirring condition. In this condition the current and time response reveals that once the potential upsurges, the current of modified elctrode is reduced, which clarifies that the poisoning of catalyst by intermediate species during the reduction process.

Based on the synthesis, characterization and discussion of the prepared materials a possible discussion and mechanism is presented. As described in the material and medthod

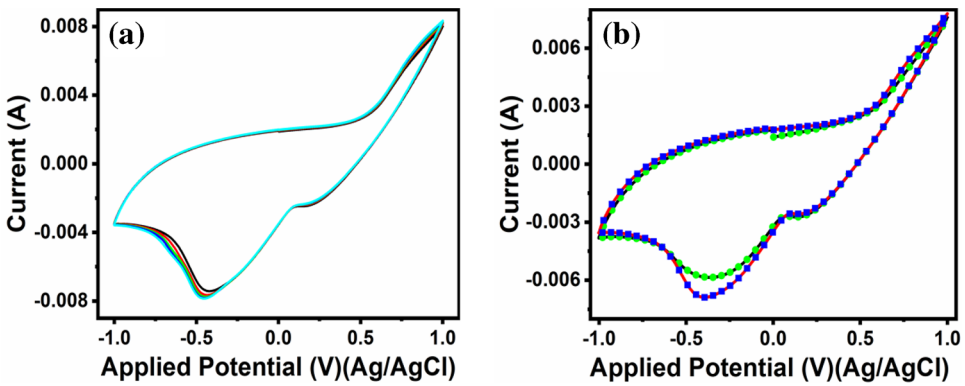

Fig. 12 **a** Five consecutive cycles of Ag-rGO nanosheets in presence of 20 mM (4-NP) in 0.1 M PBS at 100 mV/s. **b** Stability test first and after 15 days at the same conditions

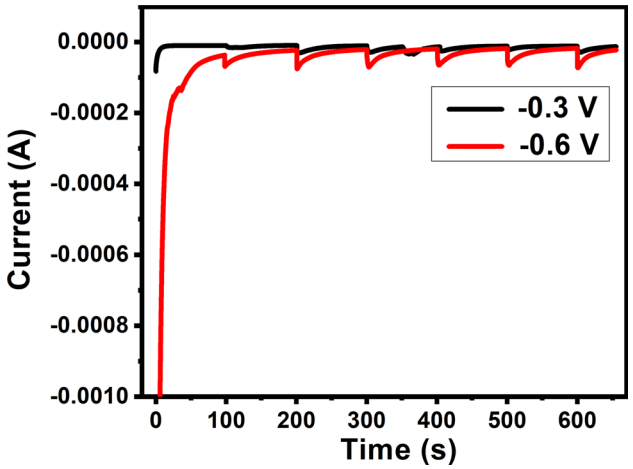

Fig. 13 Chronoamperometric current–time curve of AgNP-rGO with successive addition of 5 µL in 0.1 M PBS at − 0.3 V and − 0.6 V

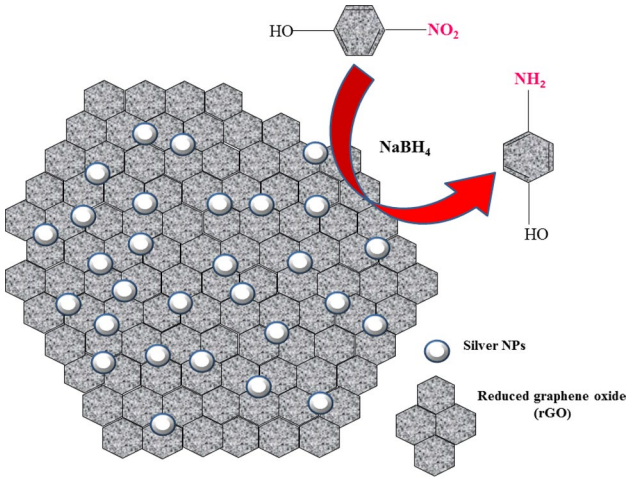

Fig. 14 Possible diagrammatic mechanism for 4-NP and AgNP-rGO

section, initally, the commecially purchased graphene oxide was reduced in a laboratory with various applied chemicals such as sodium borohydride ($NaHB_4$), monosodium di-hydrogen phos- phate (NaH_2PO_4) and disodium monohydrogen phosphate (Na_2HPO_4) etc.) and silver NPs was templated on it with the chemical modidification. The synthesized material was characterized via various techniues such as XRD for crystallinity, SEM, TEM for morphological and dimension examination of nanosheets with silver NPs. The EDS was used to know the % elemantal composition of the material, whereas other characterizations (FT-IR,TGA, Zeta and UV–Vis) were used to show the chemical characteristics of the materials (Ag-rGO). The templated silver nanoparticles on reduced graphene (Ag-rGO) were used as an electrode material to check the effeciecy against hazardous nitrophenol with three electrode system. For this, various parameters were opted to test the processed sesnsor material pasted on glassy carbon electrode (Ag-rGO/GCE). The different concentration of 4-NP (from 2 to 150 µM) was opted and analyzed the efficacy of the formed sensor. The response of current was increases with the sucessive addition of 4-NP and potential also influences. The different potential was (5 to 100 mV/s) also justifies the surfaced immobilization of the material and electrode process. The reproducibility and chronoamperometry studies well justifies the sensors applicability against the 4-NP. Its assume that during the sensing of reduced graphene sheets with silver nanoparticles the nitrophenol was converted in to the aminophenol as previous published litrature (Fig. 14) [56, 57]. This electrochemical reduction facilitates to change the hazardous material in a smaller organic molecule which are easily and detecred and degredated in liquid medium. Various other parameters which influence the study of hazardous 4-NP need to study in detail, which is in due course.

5 Conclusions

The summary of the current work shows a new synthetic Ag nanoparticles (AgNP) were utilized for to reform of a reduced graphene paste electrode (rGO). The processed materials were well scrutinized through a number of techniques for instance SEM, TEM, EDX, XRD and UV–Visible spectroscopy to identify their structural and chemical properties. The formed electrode (Ag-rGO/GCE) displays a high electrocatalytic activity towards the determination of 4-NP by significantly reducing the oxidation over potential and improving the reduction peak current. The formed electrochemical approach for rGO and Ag-rGO preparation are easy and effective for the larger scale production. The fabricated sensor exhibited good linear response, low detection limit (2 µM), high selectivity (5 to 100 mV/s, RSD) was found 2.87%) and a wide detection range (2 to 150 µM) due to the increased electrocatalytic surface area and the improved electron transferability of the graphene silver nanoparticles-hybrid nano structure. With the combination their synergistic outcome of AgNPs and rGO holds the promise for to boost the electrocatalytic performance and reduction of 4-NP. Moreover, the electrochemical sensor was applied for the detections of traces of 4-nitrophenol at a very low concentration in a very less time also it exhibit a favorable sensing performance. Therefore, these novel nano composites have great potential and could be used to fabricate sensitive sensors to detect the hazardous chemical and industrial effluents for the environment, medicine and biotechnological purposes.

Acknowledgements The authors would like to extend their sincere appreciation to the Deanship of Scientific Research at King Saud University for funding this research; Group No. (RGP-1435-078).

References

1. C. Schummer, C. Groff, J.A. Chami, F. Jaber, M. Millet, Analysis of phenols and nitrophenols in rainwater collected simultaneously on an urban and rural site in east of France. Sci. Total Environ. **407**, 5637–5643 (2009)
2. A.L. Buikema, M.J. McGimres, J. Cairns, Phenolics in aquatic ecosystems: a selected review of recent literature. Mar. Environ. Res. **2**, 87–181 (1979)
3. M.A. El Mhammedi, M. Achak, M. Bakasse, A. Chtaini, Electrochemical determi- nation of para-nitrophenol at apatite-modified carbon paste electrode: application in river water samples. J. Hazard. Mater. **163**, 323–328 (2009)
4. C. Yang, Electrochemical determination of 4-nitrophenol using a single-wall carbon nanotube film-coated glassy carbon electrode. Microchim. Acta **148**, 87–92 (2004)
5. P. Wang, J. Xiao, A. Liao, P. Li, M. Guo, Y. Xia, Electrochemical determination of 4-nitrophenol using uniform nanoparticle film electrode of glass carbon fabricated facilely by square wave potential pulses. Electrochim. Acta **176**, 448–445 (2015)
6. Z. Liu, X. Ma, H. Zhang, W. Lu, H. Ma, S. Hou, Simultaneous determination of nitrophenol Isomers based on cyclodextrin functionalized reduced graphene oxide. Electroanalysis **24**, 1178–1185 (2012)
7. Z. Liu, J. Du, C. Qiu, L. Huang, H. Ma, D. Shen, Y. Ding, Electrochemical sensor for detection of p-nitrophenol based on nanoporous gold. Electrochem. Commun. **11**, 1365–1368 (2009)
8. L. Chu, L. Han, X. Zhang, Electrochemical simultaneous determination of nitro phenol isomers at nano-gold modified glassy carbon electrode. J. Appl. Electrochem. **41**, 687–694 (2011)
9. Y. Wei, L.T. Kong, R. Yang, L. Wang, J.H. Liu, X.J. Huang, Single-walled carbon nanotube/pyrenecyclodextrin nanohybrids for ultra-highly sensitive and selective detection of p-nitrophenol. Langmuir **27**, 10295–10301 (2011)
10. X. Wang, H. Zhao, X. Quan, Y. Zhao, S. Chen, Visible light photoelectron catalysis with salicylic acid-modified TiO_2 nanotube array electrode for p-nitrophenol degradation. J. Hazard. Mater. **166**, 547–552 (2009)
11. J.A. Herrera-Melián, J.M. Dona-Rodríguez, E.T. Rendón, A.S. Vila, M.B. Quetglas, A.A. Azcárate, L.P. Pariente, Solar photocatalytic destruction of p-Nitro phenol: a pedagogical use of lab wastes. J. Chem. Educ. **78**, 775 (2001)
12. M.A. Oturan, J. Peiroten, P. Chartrin, A.J. Acher, Complete destruction of p-Nitro phenol in aqueous medium by electrofenton method. Environ. Sci. Technol. **34**, 3474–3479 (2000)
13. L. Bo, X. Quan, S. Chen, H. Zhao, Y. Zhao, Degradation of p-nitrophenol in aqueous solution by microwave assisted oxidation process through a granular activated carbon fixed bed. Water Res. **40**, 3061–3068 (2006)
14. S. Lupu, C. Lete, M. Marin, N. Totir, P.C. Balaure, Electrochemical sensors based on platinum electrodes modified with hybrid inorganic–organic coatings for determination of 4-nitrophenol and dopamine. Electrochim. Acta **54**, 1932–1938 (2009)
15. Y. Gu, Y. Zhang, F. Zhang, J. Wei, C. Wang, Y. Du, W. Ye, Investigation of photo electro catalytic activity of Cu_2O nanoparticles for p-nitrophenol using rotating ring-disk electrode and application for electrocatalytic determination. Electrochim. Acta **56**, 953–958 (2010)
16. A. Sinhamahapatra, D. Bhattacharjya, J.S. Yu, Green fabrication of 3-dimensional flower-shaped zinc glycerolate and ZnO microstructures for p-nitro phenol sensing. RSC Adv. **5**, 37721–37728 (2015)
17. G. Liu, Y. Lin, Electrochemical sensor for organophosphate pesticides and nerve agents using zirconia nanoparticles as selective sorbents. Anal. Chem. **77**, 5894–5901 (2005)
18. F.C. Moraes, S.T. Tanimoto, G.R. Salazar-Band, S.A.S. Machado, L.H. Mascaro, A new indirect electroanalytical method to monitor the contamination of natural waters with 4-nitrophenol using multiwall carbon nanotubes. Electroanalysis **21**, 1091–1098 (2009)
19. J. Zhao, L. Wei, C. Peng, Y. Su, Z. Yang, L. Zhang, H. Wei, Y. Zhang, A non enzymatic glucose sensor based on the composite of cubic Cu nanoparticles and arc- synthesized multi-walled carbon nanotubes. Biosens. Bioelectron. **47**, 86–91 (2013)
20. K. Liu, J. Zhang, G. Yang, C. Wang, J. Zhu, Direct electrochemistry and electro catalysis of hemoglobin based on poly (diallyldimethylammonium chloride) functiona -lized graphene sheets/room temperature ionic liquid composite film. Electrochem. Commun. **12**, 402–405 (2010)
21. J. Lu, I. Do, L.T. Drzal, R.M. Worden, I. Lee, Nanometal-decorated exfoliated graphite nanoplatelet based glucose biosensors with high sensitivity and fast response. ACS Nano **2**, 1825–1832 (2008)
22. O.J. Yoon, C.H. Kim, I.Y. Sohn, N.E. Lee, Toxicity analysis of graphene nanoflakes by cell-based electrochemical sensing using an electrode modified with nano composite of graphene and Nafion. Sens. Actuators **B188**, 454–461 (2013)
23. S. Alwarappan, A. Erdem, C. Liu, C. Li, Probing the electrochemical properties of graphene nanosheets for biosensing applications. J. Phys. Chem. C **113**, 8853–8857 (2009)
24. M. Zhou, Y. Zhai, S. Dong, Electrochemical sensing and biosensing platform based on chemically reduced graphene oxide. Anal. Chem. **81**, 5603–5613 (2009)
25. D. Li, M.B. Muller, S. Gilje, R.B. Kaner, G.G.N. Wallace, Processable aqueous dispersions of graphene nanosheets. Nanotechnol **3**, 101–105 (2008)
26. G. Williarris, B. Seger, P.V. Kamat, TiO_2 graphene nanocomposites UV-assisted photocatalytic reduction of graphene oxide. ACS Nano **2**, 1487–1491 (2008)
27. Q. Tang, Z. Zhou, Z.F. Chen, Graphene-related nanomaterials: tuning properties by functionalization. Nanoscale **5**, 4541–4583 (2013)
28. S. Dutta, C. Ray, S. Mallick, S. Sarkar, A. Roy, T. Pal, Au@Pd core-shell nano particles decorated reduced graphene oxide: a highly sensitive and selective platform for electrochemical detection of hydrazine. RSC Adv. **5**, 51690–51700 (2015)
29. F. Lorestani, Z. Shahnavaz, P. Mn, Y. Alias, N.S.A. Manan, One-step hydrothermal green synthesis of silver nanoparticle-carbon nanotube reduced-graphene oxide composite and its application as hydrogen peroxide sensor. Sens. Actuators B **208**, 389–398 (2015)
30. P.M. Nia, F. Lorestani, W.P. Meng, Y. Alias, A novel non-enzymatic H_2O_2 sensor based on polypyrrole nanofibers-silver nanoparticles decorated reduced graphene oxide nanocomposites. Appl. Surf. Sci. **332**, 648–656 (2015)
31. W. Liao, C. Guo, L. Sun, Z. Li, L. Tian, J. He, The electrochemical behavior of nafion/reduced graphene oxide modified carbon electrode surface and its application to ascorbic acid determination. Int. J. Electrochem. Sci. **10**, 5747–5755 (2015)
32. P.M. Nia, W.P. Meng, F. Lorestani, M.R. Mahmoudian, Y. Alias, Electrodeposition of copper oxide/polypyrrole/reduced graphene oxide as a nonenzymatic glucose biosensor. Sens. Actuators B **209**, 100–108 (2015)
33. L. Zhihua, Z. Xucheng, W. Kun, Z. Xiaobo, S. Jiyong, H. Xiaowei, M. Holmes, A novel sensor for determination of dopamine in meat based on ZnO-decorated reduced graphene oxide composites. Innov. Food Sci. Emerg. Technol. **31**, 196–203 (2015)
34. H. Ghadimi, B. Nasiri-Tabrizi, P.M. Nia, W.J. Basirun, R.A. Tehrani, F. Lorestani, Nanocomposites of nitrogen-doped graphene decorated with a palladium silver bimetallic alloy for use as a biosensor for methotrexate detection. RSC Adv. **5**, 99555–99565 (2015)

35. N.S. Ismail, Q.H. Le, H. Yoshikawa, M. Saito, E. Tamiya, Development of non-enzymatic electrochemical glucose sensor based on graphene oxide nanoribbon—gold nanoparticle hybrid. Electrochim. Acta **146**, 98–105 (2014)
36. R. Muszynski, B. Seger, P.V. Kamat, Decorating graphene sheets with gold nanoparticles. J. Phys. Chem. C **112**, 5263–5266 (2008)
37. C. Xu, X. Wang, J. Zhu, Graphene−metal particle nanocomposites. J. Phys. Chem. C **112**, 19841–19845 (2008)
38. T. Gan, J. Sun, K. Huang, L. Song, Y. Li, A graphene oxide–mesoporous MnO_2 nanocomposite modified glassy carbon electrode as a novel and efficient voltamm- etric sensor for simultaneous determination of hydroquinone and catechol. Sens. Actutators B **177**, 412–418 (2013)
39. J. Ding, S. Zhu, T. Zhu, W. Sun, Q. Li, G. Wei, Z. Su, Hydrothermal synthesis of zinc oxide-reduced graphene oxide nanocomposites for an electrochemical hydrazine sensor. RSC Adv. **5**, 22935–22942 (2015)
40. X. Huang, J. Zhang, W. Rao, T. Sang, B. Song, C. Wong, Tunable electromagnetic properties and enhanced microwave absorption ability of flaky graphite/cobalt zinc ferrite composites. J. Alloy Compd. **662**, 409–414 (2016)
41. S.K. Mishra, S.N. Tripathi, V. Choudhary, B.D. Gupta, SPR based fibre optic ammonia gas sensor utilizing nanocomposite film of PMMA/reduced graphene oxide prepared by in situ polymerization. Sens. Actutators B **199**, 190–200 (2014)
42. G. Liu, L. Wang, B. Wang, T. Gao, D. Wang, A reduced graphene oxide modified metallic cobalt composite with superior electrochemical performance for super capacitors. RSC Adv. **5**, 63553–63560 (2015)
43. K. Fatemeh, M.M. Javad, K. Samaneh, The effect of silver nanoparticles on composite shear bond strength to dentin with different adhesion protocols. J. Appl. Oral Sci. **25**, 367–373 (2017)
44. T. Qiu, J.G. Yang, X.J. Bai, Y.L. Wang, The preparation of synthetic graphite materials with hierarchical pores from lignite by one-step impregnation and their characterization as dye absorbents. RSC Adv. **9**, 12737–12746 (2019)
45. N.I. Kovtyukhova, P.J. Ollivier, B.R. Martin, T.R. Mallouk, S.A. Chizhik, E.V. Buzaneva, A.D. Gorchinskiy, Layer-by-layer assembly of ultrathin composite films from micron-sized graphite oxide sheets and polycations. Chem. Mater. **11**, 771–778 (1999)
46. S. Ameer, I.H. Gul, N. Mahmood, M. Mujahid, Semiconductortometallic flipping in a $ZnFe_2O_4$–graphene based smart nanosystem: temperature/microwave magneto dielectric spectroscopy. Mater. Charact. **99**, 254–265 (2015)
47. J. Li, C.Y. Liu, Ag/graphene heterostructures: synthesis, characterization and optical properties. Eur. J. Inorg. Chem. **8**, 1244–1248 (2010)
48. S. Raja, V. Ramesh, V. Thivaharan, Green bio synthesis of silver nanoparticles using *Calliandra haematocephala* leaf extract, their antibacterial activity and hydrogen peroxide sensing capability. Arab. J. Chem. **10**, 253–261 (2017)
49. L. Lin, P. Qiu, X. Cao, L. Jin, Colloidal silver nanoparticles modified electrode and its application to the electroanalysis of cytochrome c. Electrochim. Acta **53**, 5368–5372 (2008)
50. R. Shankar, A. Karthil, A. Prabu, S. Karthik, K.S. Shivashangari, V. Ravikumar, *Origanum vulgare* mediated biosynthesis of silver nanoparticles for its antibacterial and anticancer activity. Colloids Surf. B **108**, 80–84 (2013)
51. M. Haneef, H. Saleem, A. Habib, Use of graphene nanosheets and barium titan- ate as fillers in PMMA for dielectric applications. Synth. Met. **223**, 101–106 (2017)
52. M.A. Worsley, P.J. Pauzauskie, T.Y. Olson, J. Biener, J.H. Satcher, J.T.F. Baumann, Synthesis of graphene aerogel with high electrical conductivity. J. Am. Chem. Soc. **132**(40), 14067–14069 (2010)
53. P. Rameshkumar, R. Ramaraj, Electroanalysis of nitrobenzene derivatives and nitrite ions using silver nanoparticles deposited silica spheres modified electrode. J. Electroanal. Chem. **731**, 72–77 (2014)
54. K. Giribabu, R. Suresh, R. Manigandan, S. Munusamy, S.P. Kumar, S. Muthamizh, V. Narayanan, Nanomolar determination of 4-nitrophenol basedon a poly (methylene blue) modified glassy carbon electrode. Analyst **138**, 5811–5818 (2013)
55. Y. Bai, Y. Du, J. Xu, H. Chen, Choline biosensors based on a bi-electrocatalytic property of MnO_2 nanoparticles modified electrodes to H_2O_2. Electrochem. Commun. **9**, 2611–2616 (2007)
56. N.I. Ikhsan, P. Rameshkumar, N.M. Huang, Controlled synthesis of reduced graphene oxide supported silver nanoparticles for selective and sensitive electro chemical detection of 4-nitrophenol. Electrochim. Acta **192**, 392–399 (2016)
57. A.T.E. Vilian, S.R. Choe, K. Giribabu, S.C. Jang, C. Roh, Y.S. Huh, Y.K. Han, Pd nanospheres decorated reduced graphene oxide withmulti-functions: highly efficient catalytic reduction and ultrasensitivesensing of hazardous 4-nitrophenol pollutant. J. Hazard. Mater. **333**, 54–62 (2017)